

parent, is compatible with our data on account of its width (see Table I). This is demonstrated in Fig. 3 which shows the contributions of each term to the best fit to our data. The higher-mass region is fitted with a general polynomial in mass squared; only the linear and cubic terms were needed.

(3) The combination of the good resolution of the apparatus and the high statistics of the data makes it possible to place limits on the cross sections of bumps which were not seen. From an examination of the mass plot of our data, it is clear that we have no evidence for any narrow resonances (except those listed in Table I) produced with cross sections comparable to 25% that of the  $\xi(953)$  [i.e., with  $(d\sigma/d\Omega)_{c.m.}$  greater than  $5 \times 10^{-36} \text{ cm}^2/\text{sr}$ ] in the mass region to 1.1 GeV<sup>2</sup>.

We would like to thank Dr. R. A. Schluter for his contribution during the early phases of the experiment, Dr. E. Ellis and Mr. R. Gore for their aid in data analysis, and particularly Dr. J. Norem and the staff of the Princeton-Pennsylvania Accelerator for their support.

\*Research supported in part by the U. S. Atomic Energy Commission (University of Pennsylvania Group) and the National Science Foundation (Rutgers University Group).

†Now at Rutherford High Energy Laboratory, Chilton, Didcot, Berkshire, England.

<sup>1</sup>H. Brody *et al.*, Phys. Rev. Lett. **24**, 984 (1970). The ordinate of Fig. 1 was mislabeled; it should read 1 through 5 (rather than 0.1 through 0.5). The  $d\sigma$  values in Table I are correct.

<sup>2</sup>E. Groves, Ph.D. thesis, University of Pennsylvania, 1970 (unpublished).

<sup>3</sup>See Eq. (4) in B. Maglič and G. Costa, Phys. Lett. **18**, 185 (1965).

<sup>4</sup>M. Aguilar-Benitez *et al.*, Phys. Rev. Lett. **25**, 1635 (1970).

<sup>5</sup>J. Rosner and E. Colglazier, Phys. Rev. Lett. **26**, 933 (1971).

<sup>6</sup>S. Barshay, Princeton-Pennsylvania Accelerator Report No. 23, 1969 (unpublished) (also reproduced in Ref. 2, above), predicts on the basis of our observed  $\pi^0$ -to- $\eta^0$  production ratio and the  $\eta$ - $\eta'$  mixing angle 4 times more  $\eta'$  production than  $\pi$  production in our experiment. Our data give a maximum  $\eta'$  production only one quarter as large as  $\pi$  production.

## Prism Plot: A New Analysis of Multibody Final States\*

J. E. Brau,† F. T. Dao, M. F. Hodous, I. A. Pless, and R. A. Singer

Massachusetts Institute of Technology, Cambridge, Massachusetts 02139

(Received 9 July 1971)

We present a new technique for analyzing multibody states. This analysis makes possible the selection of samples of events that contain only resonances, particle correlations, or phase space. A unique feature of this analysis is that every event in the data is assigned to a particular sample. The three-body final state  $\pi^+ + p \rightarrow p + \pi^+ + \pi^0$  is analyzed as an example.

In this Letter we present a technique for analyzing multibody final states. The bases of this analysis are the Van Hove<sup>1</sup> angular variables and an  $N$ -dimensional energy simplex. The underlying concept is an attempt to utilize a complete set of parameters to analyze the final states. Given an unpolarized beam and target and an  $N$ -body final state, there are  $3N - 5$  free parameters required to specify that final state completely. We define  $2N - 2$  parameters that form a generalized equilateral rectangular prism. In addition, we define the remaining  $N - 3$  required parameters in a manner useful for specific problems.

We will use the previously published  $\pi^+ + p$  data<sup>2</sup> at 3.9 GeV/c as an example. For  $N=3$  we need four parameters. The first parameter which we choose is the well-known Van Hove angle.<sup>1</sup> Fig-

ure 1(a) gives our representation of this angle in a manner useful for generalizing to higher dimensions; namely, the  $N$  unit longitudinal momentum vectors lie in  $(N-1)$ -dimensional space in such a way that any two of them form an angle with each other such that the cosine of this angle is equal to  $-1/(N-1)$ . Therefore, we have defined the Van Hove angle ( $\theta$ ) so that baryons produced with positive center-of-mass longitudinal momenta are in the angular region  $0^\circ \leq \theta \leq 180^\circ$ .

Our second parameter is  $R/R_{\max}$ , which is the ratio of the length of the radius vector in the Van Hove plot to the maximum length that vector could have at the given Van Hove angle [Fig. 1(b)]. If  $R/R_{\max} = 0$ , the event lies in a plane perpendicular to the incident direction, and if  $R/R_{\max} = 1$ , the event is collinear with the incident direction.

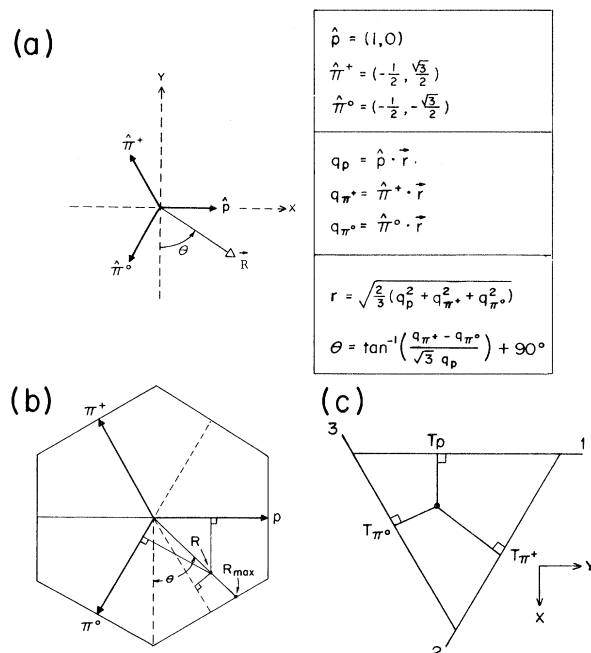


FIG. 1. (a) Definition of three-body Van Hove angle. (b) Van Hove hexagon and definition of  $R_{\max}$ . (c) Dalitz-Fabri plot; two-dimensional energy simplex. The numbers 1, 2, and 3 identify each edge.

Our final two variables are the total energy of the proton and  $\pi^+$ . These energy variables can best be represented by a point in an energy equilateral triangle (two-dimensional simplex) as was done by Fabri and Dalitz [Fig. 1(c)]. If we use the Van Hove angle as a coordinate together with the two-dimensional energy simplex, we can construct a data plot bounded by a rectangular equilateral prism. The outline of such a prism is shown in Fig. 2(a), illustrating the reason for calling this method prism plot analysis. However, the complete prism includes  $R/R_{\max}$ .

Each event will appear in this plot as a single point. Figures 2(a) and 2(b) show the complete prism plot populated with Monte Carlo phase-space events, and Figs. 2(c) and 2(d) populated with the 3.9-GeV/c  $\pi^+ + p$  data. Figures 2(b) and 2(d) are the respective  $R/R_{\max}$  distributions. The striking features of the 3.9-GeV data are the peaking of  $R/R_{\max}$  near 0.9, and the accumulation of the data into three distinct tubes in the upper half of the prism. As we will demonstrate, each tube contains a single resonance, or two-body correlation. One can show that this clustering is a reflection of the following two empirical observations: (1) The transverse momentum of any individual particle is limited ( $\sim 0.4$  GeV/c). (2) The  $Q$  value in the center of mass is of the

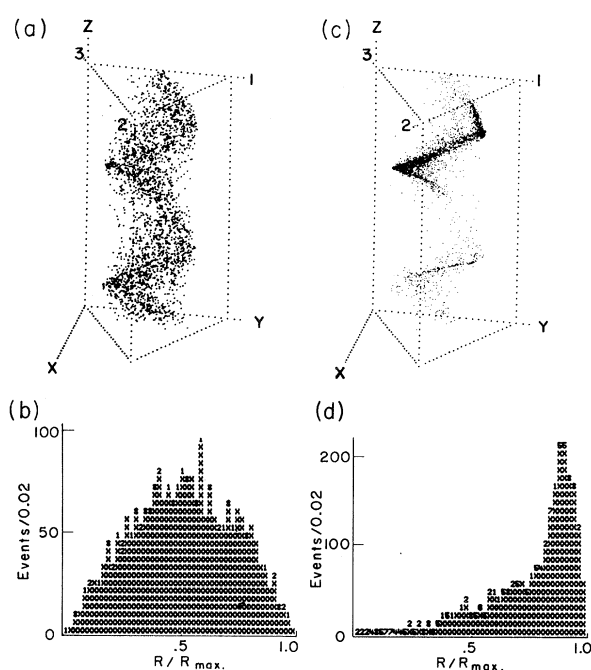


FIG. 2. (a) Three-body prism plot for 3.9-GeV/c  $\pi^+ + p$  invariant phase-space Monte Carlo events. The numbers 1, 2, and 3 are the same as in Fig. 1(c). The  $x$  and  $y$  axes are the same as Fig. 1(c). The  $z$  axis is the Van Hove angle  $\theta$ . (b)  $R/R_{\max}$  distribution for 3.9-GeV/c  $\pi^+ + p$  invariant phase-space Monte Carlo events. (c) Three-body prism plot for 3.9-GeV/c  $\pi^+ + p \rightarrow p + \pi^+ + \pi^0$  data. Various portions of prism plot represent different physical processes. (d)  $R/R_{\max}$  distribution for 3.9-GeV/c  $\pi^+ + p \rightarrow p + \pi^+ + \pi^0$  data.

same order as the mass of any correlated system in the final state. If these two conditions are met for any multibody final state, kinematics require this clustering.

The three-body final state can be any of the following:

$$\pi^+ + p \rightarrow \Delta^{++} + \pi^0, \quad (1)$$

$$\rightarrow \Delta^+ + \pi^+, \quad (2)$$

$$\rightarrow p + \rho^+, \quad (3)$$

$$\rightarrow (p\pi^0) + \pi^+ \text{ (diffraction dissociation)}, \quad (4)$$

$$\rightarrow p + \pi^+ + \pi^0 \text{ (phase space)}. \quad (5)$$

Comparing  $R/R_{\max}$  in Figs. 2(b) and 2(d), one sees immediately that three-body phase space plays almost no role in this reaction.

In the following discussion we limit ourselves to these events in Fig. 2(c) which make up the upper half of the prism. These events are contained in three distinct tubes—the upper tube, the central tube, and the lower tube. Although it is not clear in this figure, the lower tube is actu-

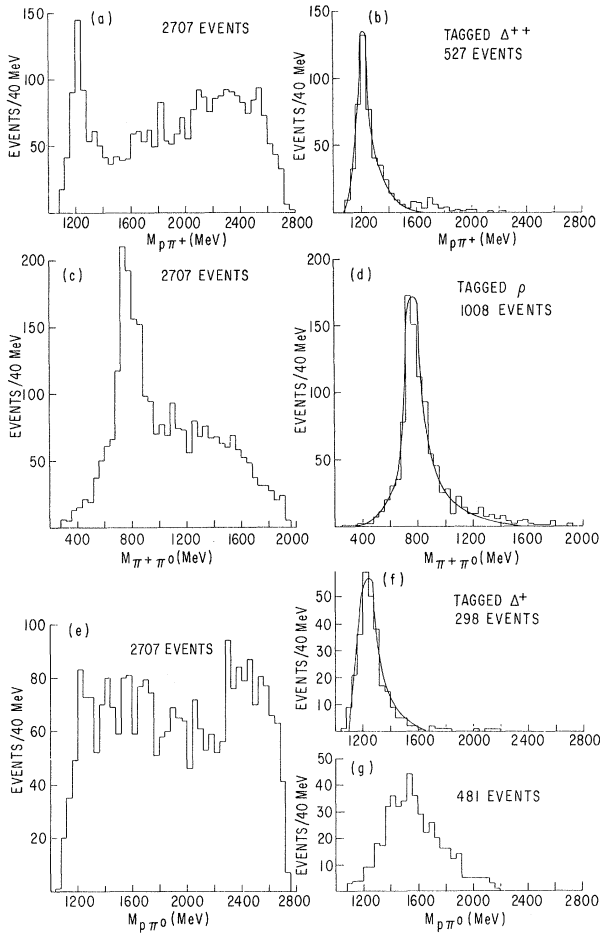


FIG. 3. (a) Invariant mass of  $p\pi^+$ , all events. (b)  $M(p\pi^+)$  ( $\Delta^{++}$ ) from prism plot analysis. The solid curve is the best resonance fit. (c) Invariant mass of  $\pi^+\pi^0$ , all events. (d)  $M(\pi^+\pi^0)$  ( $\rho^+$ ) from prism plot analysis. The solid curve is the best resonance fit. (e) Invariant mass of  $p\pi^0$ , all events. (f)  $M(p\pi^0)$  ( $\Delta^+$ ) from prism plot analysis. The solid curve is the best resonance fit. (g)  $M(p\pi^0)_{dd}$  from prism plot analysis. The adjective "tagged" on some plots indicate that the events displayed are contained in specific regions of the prism plot.

ally two tubes which can be distinguished from each other by properly rotating the prism.

Figure 3(a) gives the  $p\pi^+$  invariant mass distribution for our total sample and Fig. 3(b) that for the upper tube in the prism plot. The curve in Fig. 3(b) is the resonance shape giving the best fit. This is only one indication that this tube is populated only by the reaction  $\pi^+ + p \rightarrow \Delta^{++} + \pi^0$ . Figure 3(c) gives the  $\pi^+\pi^0$  invariant-mass distribution for all our data and Fig. 3(d), that for the central tube of the prism plot. The curve in Fig. 3(d) is the resonance shape giving the best fit.

TABLE I. Cross sections for 3.9-GeV/c  $\pi^+ + p \rightarrow p + \pi^+ + \pi^0$  (2291 events).

Final states	$\sigma$ (mb)	%
$p\rho^+$	$0.85 \pm 0.04$	44
$\Delta^{++}\pi^0$	$0.42 \pm 0.03$	22
$\Delta^+\pi^+$	$0.23 \pm 0.04$	12
$(p\pi^0)_{dd}\pi^+$	$0.40 \pm 0.05$	20
Phase space	$0.04 \pm 0.02$	2

This is only one indication that this tube is populated only by the reaction  $\pi^+ + p \rightarrow p + \rho^+$ . Figure 3(e) is the  $p\pi^0$  invariant mass distribution for all our data, Fig. 3(f), that for one of the lower tubes, and Fig. 3(g), that for the second of the lower tubes in the prism plot. The curve in Fig. 3(f) is the best-fit resonance shape while Fig. 3(g) is a histogram of events which we call diffraction dissociation (dd). This is only one indication that the lower tubes contain only the two reactions

$$\pi^+ + p \rightarrow \Delta^+ + \pi^+, \quad \pi^+ + p \rightarrow (p\pi^0)_{dd} + \pi^+.$$

In all the above samples, the "wrong pairing" of particles shows no resonances, and all Gottfried-Jackson distributions are smooth and symmetrical. The production and decay angular distributions for the  $\Delta^{++}$  and the  $\Delta^+$  are the same. The ratio  $\Delta^{++}/\Delta^+ = \frac{3}{4}$  is as required by isospin invariance. The cross sections for the final states are given in Table I. The errors are statistical only and do not include possible systematic uncertainties of the prism plot method. Table I shows that the final state  $\pi^+ + p \rightarrow p + \pi^+ + \pi^0$  is all quasi two-body. There have been indications of this in previous work.<sup>2</sup>

We will now generalize this technique to the four-body final state. Figure 4(a) gives our four-body Van Hove plot while Fig. 4(b) is the three-dimensional energy simplex, a tetrahedron. One of the properties of an  $N$ -dimensional simplex is that the sum of the perpendicular distances from an internal point to all faces is a constant. The three-dimensional simplex plus the two Van Hove angles  $\theta_1$  and  $\theta_2$  generate a five-dimensional prism. The three kinetic energies, the two Van Hove angles, and  $R/R_{\max}$  specify our  $2N-2$  variables for this four-body case. All two-body final-state correlations will populate planes in the energy simplex. This is again a consequence of the two empirical observations mentioned above.

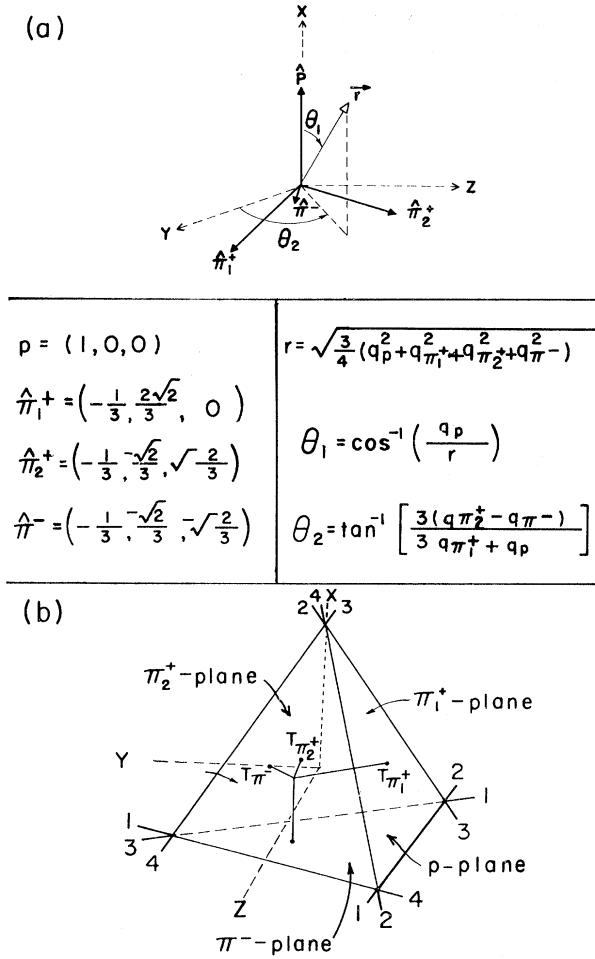


FIG. 4. (a) Definition and convention of four-body Van Hove angles. (b) Four-body kinetic-energy simplex. The numbers 1, 2, 3, and 4 identify each face. For example, the  $\pi^-$  plane is the 4-face as the three edges of this face are labeled 4.

Figures 5(a)–5(c) show the prism plot populated by invariant phase space, while Figs. 5(d)–5(f) show the prism plot populated by our four-body  $\pi^+ + p$  data at 3.9 GeV/c. Again, a glance at  $R/R_{\max}$  indicates that phase space plays a small role in this reaction, and other regions of the prism plot show definite clusterings. Again, as stated above, these clusterings must contain final-state correlations. As we will show in a more complete paper, the separation of the constituents of these final states is just as dramatic as in the three-body case. In the four-body case, the prism plot lacks one variable of the number required to form a complete set. We have found it convenient to use an invariant mass for this variable. In particular, for this final state, we use the  $\pi^+\pi^+$  invariant mass since we find this in-

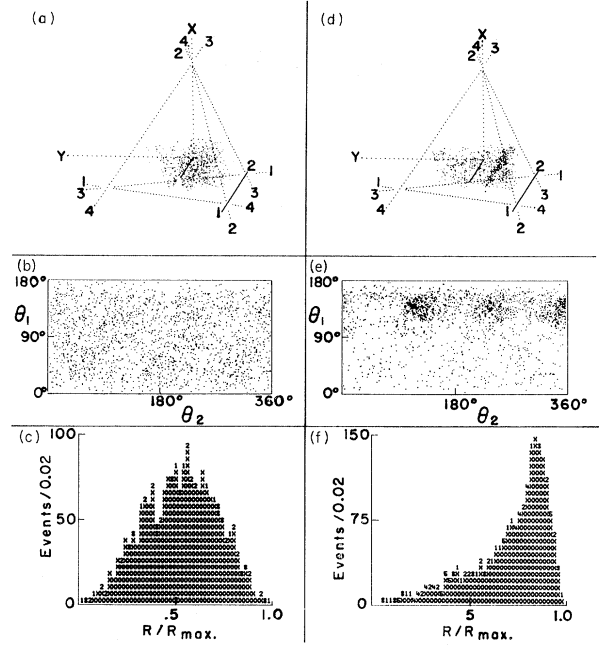


FIG. 5. (a) Four-body kinetic-energy simplex for 3.9-GeV/c  $\pi^+ + p \rightarrow p + \pi^+ + \pi^+ + \pi^-$  invariant phase-space Monte Carlo events. The numbers 1, 2, 3, and 4 and the  $x$ ,  $y$ , and  $z$  axes are the same as in Fig. 4(b). (b) Four-body Van Hove angular plot for invariant phase-space Monte Carlo events. (c)  $R/R_{\max}$  distribution for invariant phase-space Monte Carlo events. (d) Four-body kinetic-energy simplex for 3.9-GeV/c  $\pi^+ + p \rightarrow p + \pi^+ + \pi^+ + \pi^-$  data. (e) Four-body Van Hove angular plot for 3.9-GeV/c  $\pi^+ + p \rightarrow p + \pi^+ + \pi^+ + \pi^-$  data. (f)  $R/R_{\max}$  distribution for 3.9-GeV/c  $\pi^+ + p \rightarrow p + \pi^+ + \pi^+ + \pi^-$  data.

variant mass contains no resonant shapes and, therefore, cannot be a source of bias in the analysis.

The generalization to  $N$  bodies is straightforward.<sup>3</sup> The  $N$ -dimensional Van Hove angles are characterized by  $N$  equally spaced unit vectors in an  $(N-1)$ -dimensional simplex. We have found it convenient to use invariant masses to complete the set of parameters.

We would like to thank Dr. Vera Kistiakowsky for stimulating discussions and helpful suggestions on this work.

\*Work supported in part through funds provided by the U. S. Atomic Energy Commission under Contract No. AT(30-1) 2098.

†Present address: Holloman Air Force Base, N. Mex. 88330.

<sup>1</sup>L. Van Hove, Phys. Lett. **28B**, 429 (1969), and Nucl.

Phys. B9, 331 (1969).

<sup>2</sup>P. L. Bastien *et al.*, Phys. Rev. D 3, 2047 (1971).

<sup>3</sup>Complete details of this generalization are available

in F. T. Dao, M. R. Hodous, I. A. Pless, and R. A.

Singer, Massachusetts Institute of Technology PEPR P

Programming Note—Physics 101, 1971 (unpublished).

---

## ERRATA

---

### SELECTION RULE FOR $\Sigma^+ \leftrightarrow \Sigma^-$ TRANSITIONS IN ELECTRON-MOLECULE COLLISIONS.

D. C. Cartwright, S. Trajmar, W. Williams, and  
D. L. Huestis [Phys. Rev. Lett. 27, 704 (1971)].

The scattered electrons were collected in an  
angular region of  $4^\circ$ , *not*  $40^\circ$ , as incorrectly  
printed in the fifth line, first column, of page  
705.

### ELECTRONIC RECOMBINATION COEFFICIENT OF MOLECULAR HELIUM IONS. A. Wayne John- son and J. B. Gerardo [Phys. Rev. Lett. 27, 835 (1971)].

The smaller sized numbers listed under  $\alpha$  in  
Table I and in the two equations on page 838  
should not have + and – signs. These numbers  
are the upper and lower limits of our measure-  
ments. Immediately following the equations on  
page 838, please read, “where the limits quoted  
...”